Research Square

Preprints are preliminary reports that have not undergone peer review.
They should not be considered conclusive, used to inform clinical practice,
or referenced by the media as validated information.

Design and Experimental Investigation of a Curved -Plate Drag Turbine for Electricity Generation While Changing the Electrical Load on The Performance from Wasted Air Pressure

Mohamed A. Mosbah

mohammed_abdulrahman@techedu.sohag.edu.eg

Sohag University

Khalil Ibrahim

Assiut University

Hamdy Abo El Daheb

Sohag University

Article

Keywords: Curved-plate drag turbine, Waste air pressure, Compressed air energy recovery, Electricity generation, Experimental investigation, Pneumatic energy, Energy conversion

Posted Date: November 23rd, 2026

DOI: https://doi.org/10.21203/rs.3.rs-11578540/v1

License: This work is licensed under a Creative Commons Attribution 4.0 International License.
Read Full License

Additional Declarations: No competing interests reported.

Design and Experimental Investigation of a Curved -Plate Drag Turbine for Electricity Generation While Changing the Electrical Load on The Performance from Wasted Air Pressure

Mohamed A. Mosbah[1, *], Khalil Ibrahim[2,3], and Hamdy Abo El Daheb[4]

[1]Electric power Technology Department, Faculty of Technology and Education, Sohag University, Sohag 82524, Egypt.

[2]Professor of Mechatronics Department -Faculty of Engineering Assiut University, [3] Dean of Faculty of Industry and Energy Technology-New Assiut Technological University.

[4]Automotive Technology Department, Faculty of Technology and Education, Sohag University, Sohag, Egypt.

[*]corresponding author: mohammed_abdulrahman@techedu.sohag.edu.eg

Abstract: With a focus on the impact of electrical loads on turbine performance, this paper describes the design and experimental analysis of a Curved -plate drag turbine for the production of energy from lost air pressure. The suggested method uses a mechanical turbine-generator configuration to recapture otherwise lost pneumatic energy and transform it into usable electrical energy. In order to interact with the incoming waste-air stream and generate rotational motion, the turbine is made up of many Curved plates stacked inside a specifically made housing. To examine the turbine's performance under various electrical load scenarios while preserving regulated waste-air pressure and operating parameters, an experimental test rig was created. Important variables were monitored for various electrical loads throughout the studies, such as turbine rotational speed, produced voltage, electrical current, and output power. The operational parameters and energy-conversion behavior of the suggested system were determined by analyzing the impact of increasing electrical load on turbine rotational speed and electrical power output. The electrical load significantly affects turbine speed, produced voltage, current, and power, according to the experimental results, which also illustrate the link between mechanical loading and electrical output. The suggested system offers a straightforward method for recovering energy from pneumatic pressure or wasted compressed air and turning it into electrical energy. According to the testing results, under various load situations, which rose from 0.56 W to 2.45 W, the produced voltage climbed from 1.18 V to 4.87 V while the average rotational speed increased from 1015.38 rpm to 1200 rpm. The results offer a foundation for adjusting the electrical loading conditions, operating pressure, and Curved-plate turbine design to enhance energy recovery and system performance. This method might be used in pneumatic equipment, industrial compressed air systems, and other systems that release pressured air as waste.

Keywords: Curved-plate drag turbine, Waste air pressure, Compressed air energy recovery, Electricity generation, Experimental investigation, Pneumatic energy, Energy conversion.

1. Introduction:

One of the most crucial systems in the air brake circuits of trucks and train tractors is the air circuit, which is used to run the braking system as well as numerous insulation systems, automated doors, and alarm horns. The compressor, which compresses the air and transfers it to the other circuit components, is the system's beating heart. In the field of mechanical and energy engineering, compressed air, also referred to as pneumatics, is one of the most popular mediums for energy conversion and transmission. This science is crucial to many industrial applications,

including pneumatic control systems, robotics, production lines, railroads, and even alternative power generation processes, because it uses the compressible and expandable qualities of air to produce the necessary motion and force. The Tesla turbine stands out as a creative and practical option among the promising technologies that use compressed air to generate electricity. This turbine, which was created by Nikola Tesla in the early 20th century, has a special operating mechanism based on viscosity and friction instead of the conventional blades seen in other turbines. Compressed air can be used to recover wasted energy in railroad and industrial systems because it efficiently transforms air energy into mechanical energy when it passes through closely spaced disks inside the turbine.

A step toward creating sustainable solutions to more effectively utilize energy is the integration of Tesla turbine technology with pneumatic systems. This untapped energy can be transformed into an effective source for producing power or running different machinery by using compressed air that is lost in rail systems or industries. In order to take advantage of the air energy or unused air pressure that results from the operation of the train or truck's mechanical compressor, which is mechanically connected to the engine, design and implement a novel secondary circuit within the air system in trucks and trains that uses compressed air in the brake system. The compressor typically charges the air tank used in the brake system. When the pressure reaches the necessary level, it stops pumping air into the main circuit, but because it is mechanical and is fed directly from the train or truck's engine or transmission system, its kinetic energy keeps working without producing any useful load. Figure 1 shows the air brake system with tesla turbine. Many previous studies have examined the Tesla turbine through design, the effect of air pressure on the internal blades, or the change in the design of its internal blades.

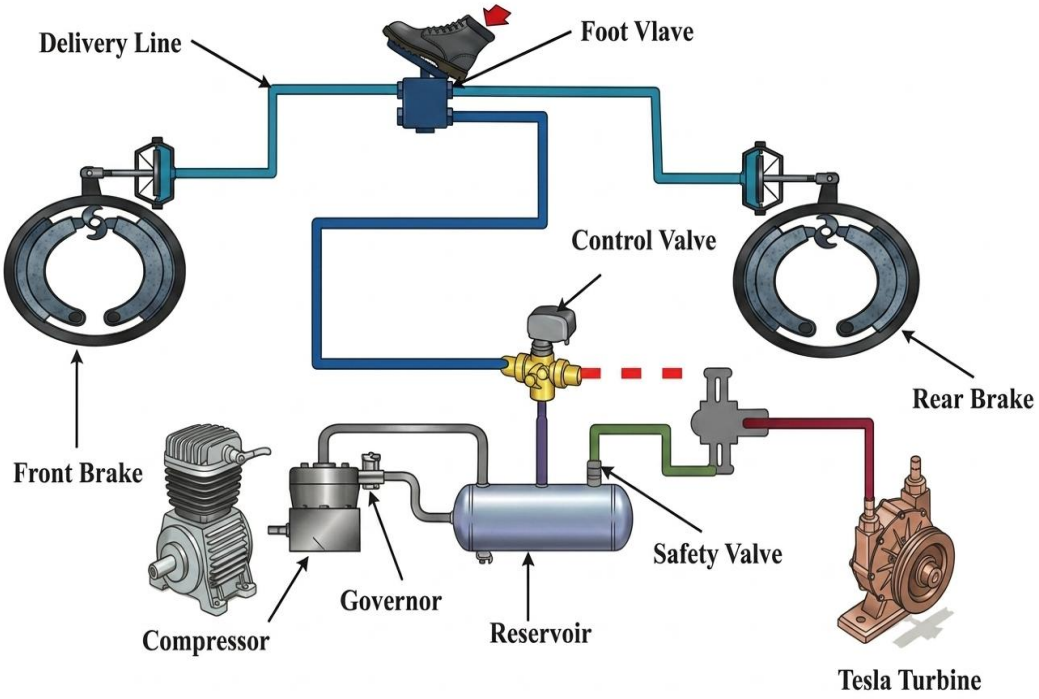

Figure 1. Air brake system with tesla turbine.

Following an initial examination of the fundamental operational features of the Tesla turbine [1] 787 watts of output power and 32.1% efficiency were achieved structural parameters, including nozzle height, width, and disk spacing, were optimized. The Tesla turbine produced 787 watts of output power and 32.1% efficiency after a thorough tuning process. Five common wet operating fluids (R22, R417a, R134a, R152a, and R290) were chosen to examine their impact on the thermal performance of a Tesla turbine and an organic Rankine (ORC) system using a thermodynamic model constructed [2]. When various wet working fluids were utilized in the organic Rankine cycle system, the impact of modifications to the primary structural parameters of the Tesla turbine on the system's and the turbine's performance was also examined. According to the findings, when R22 was used as the operating fluid under design conditions, the maximum turbine efficiency was 42.0%. A novel trans critical carbon dioxide heat pump cycle in which the expansion valve is replaced by a Tesla turbine [3]. The movement of carbon dioxide inside a Tesla turbine is first simulated using a 3D computational fluid dynamics model. The collected findings are then used as data for thermodynamic modeling of the heat pump cycle. Additionally, the turbine power reaches its maximum at a rotor angular velocity of 1000 rad/s; thus, raising the inlet pressure increases torque, which in turn increases turbine power. As a function of rotor angular velocity, a thermodynamic trade-off is shown between the power output from the Tesla turbine and the vapor quality at the turbine's outlet. The maximum exergy efficiency of the Tesla turbine, which in turn results in the maximum coefficient of performance of the entire cycle, is correlated with the optimal rotor angular velocity, as demonstrated numerically.

Numerical and analytical research has been done on the Tesla turbine with insulated rotors for waste heat recovery in Rankine cycle power plants [4]. To investigate the thermos fluid dynamics and performance characteristics for a variety of dimensional and dimensionless parameters, simulations are run for the multiphase, compressible, turbulent flow of wet steam. The efficiency curves are contrasted with those of the laminar, incompressible air flow, which appears to follow a similar qualitative pattern but has a much smaller inlet angle effect. An intriguing initial cost reduction is seen in the fuel cost estimation of a power plant using Tesla turbines that use bled steam. The performance characteristics of a Tesla turbine, a novel bladeless expander integrated into an ORC system working under low-grade temperature settings (90–130 ◦C), were thoroughly investigated experimentally [5]. To rigorously assess the turbine's isentropic efficiency, dynamic interactions with system parameters, and related mechanical losses, a prototype tiny ORC system with a Tesla turbine-generator assembly was created. With a thorough examination of the system's heat absorption properties, the testing results show that the Tesla turbine achieves an impressive peak isentropic efficiency of 62.28% and produces a maximum output power of 31.76 W under the evaluated conditions.

Constructed a small-scale experimental model of an air-powered Tesla turbine to verify the findings of the SLR investigation [6]. To determine the impact of independent variables on turbine output power and mechanical efficiency, the Design of Experiments (DoE) methodology was utilized. For the prototype with an output capacity of less than 1 kW, the inlet air pressure, temperature, and rotation speed were selected as variable elements in a composite central design. The findings show that an average increase of 1 bar in inlet pressure resulted in a 5% increase in efficiency. Simulations in the SLR study revealed an average efficiency of 40% to 60%, whereas experimental tests reported an average maximum efficiency of 20%. A model for examining the flow inside Tesla turbine parts that accounts for the rotor walls' roughness was given [7]. To

achieve the required reduction in the non-dimensional velocity curve, the model modifies the dynamic viscosity in the governing equations using the equivalent sand grain approach. To account for the change in the radial velocity's form, a quasi-experimental function has been developed. Although the turbine's overall performance improves, the flow channels inside the rotor become less rough. In comparison to a smooth rotor, a roughness of 10^{-3} meters improved the generating power and equal entropy efficiency by coefficients of 2.5 and 3, respectively. In order to answer two basic research questions [8] and associates investigated the integration of a bladeless Tesla turbine rotor with an axial-flow permanent magnet (AFPM) electric machine: first, the viability of creating a small-scale power generation device (roughly 5–15 watts); and second, the applicability of the same principle to create a gas heater that operates during expansion from high pressure (e.g., from 1.2 MPa to atmospheric pressure). The findings demonstrate the integrated system's potential benefits in terms of its useful applications and space-saving architecture. The potential application of this idea in small-scale distributed energy systems is encouraging.

To validate the porous medium layer (PML) concept [9] conducted experimental testing on a tiny channel. The model was then used to analyze a Tesla turbine. Large vortex simulation findings for the case of smooth rotor walls confirmed that the turbulence closure model was the k-ω shear stress transfer model. The impact of roughness height on turbine efficiency and flow coefficients was investigated by testing three distinct porous layer heights, each with adjusted coefficients. The study showed that the porous medium layer roughness model adequately models the performance of a Tesla turbine in the studied situations and appropriately depicts the genuine effect of roughness on flow. Thorough experimental research on the impact of different operating conditions on the efficiency of Tesla turbines was provided [10]. Water was utilized as the operating fluid in a bladeless turbine with nine disks and four inlets. The number of turbine inlets, mass flow rates, and nozzle angles were among the factors examined. According to the study, turbine efficiency rises with fewer nozzle angles and more turbine inlets. It has been noted that when the number of turbine inlets rises, nozzle angle becomes a crucial factor. When the running fluid entered the turbine through two nozzles at a 7-degree angle, efficiencies of up to 78% were attained.

A thorough experimental analysis of the performance characteristics of the Tesla turbine, a novel bladeless turbine incorporated into the organic Rankine cycle (ORC) system working in low thermal settings (90–130 degrees Celsius) [11]. To rigorously assess the turbine's isentropic efficiency, its dynamic interactions with system parameters, and related mechanical losses, a small prototype of an organic Rankine cycle (ORC) system consisting of a Tesla turbine and a generator was created. With a thorough examination of the system's heat absorption characteristics, experimental results demonstrate that the Tesla turbine achieves an impressive peak isentropic efficiency of 62.28%, producing a maximum output power of 31.76 watts under the studied conditions. The Tesla turbine, which is renowned for its affordability and ease of use, was employed as an expansion device [12]. To assess a Tesla pneumatic turbine's performance, a performance tester was created. Three factors were analyzed in the experimental studies: the torque control current range of 20 to 100 mA, the inlet temperature range of 35 to 80 degrees Celsius, and the inlet pressure range of 0.45 to 0.8 MPa. Furthermore, efficiency was greatly increased at higher temperatures. When the temperature rises above 60 degrees Celsius at a pressure of 0.6 MPa and a current of 80 mA, the isentropic efficiency climbs dramatically to 14%, which is almost three times higher than the performance at 35 degrees Celsius.

Suggested considering important operating characteristics such rotation speed, inlet pressure, and mass flow rate in addition to the output power and isentropic compression efficiency as ideal target parameters [13]. Subsequent studies of structural parameters, such as nozzle height and width, distance between disks, disk thickness, disk diameter, and number of disks, were conducted after an initial examination of the fundamental operational characteristics of the Tesla turbine. The Tesla turbine produced an output power of 787 watts and an efficiency of 32.1% after a thorough tuning process. Based on an air motor [14] constructed an experimental compressed air platform and carried out integrated experiments to compress and expand this motor. It examined how important factors like speed, torque, and current affected the air motor's performance in various operating modes, serving as a guide for the use and advancement of compact compressed air energy storage devices. According to the data, the motor's overall efficiency reaches 14.01% in expansion mode, and its output power reaches 1257.87 watts. This mode achieves a certain cooling effect while concentrating on high power output and cost-effective operation within an average range of rotational speed and current. A thorough evaluation of the present state and potential future directions of Tesla turbine utilization in waste heat recovery applications is given [15]. The study highlights the benefits and drawbacks of Tesla turbines while introducing them and their working principles. Additionally, it offers an overview of published studies on the application of Tesla turbines to recover waste heat in a variety of industrial sectors, such as manufacturing, power plants, the automotive industry, and renewable energy systems. The study assesses Tesla turbines' energy conversion efficiency and performance critically. The technological difficulties and obstacles related to using Tesla turbines to recover waste heat are also covered in this study.

This research project focuses on the design, construction, and practical experimentation of a bladeless Tesla central turbine for electrical power generation [16]. SolidWorks design software, fluid dynamics principles, and machine element design were employed to guarantee the best mechanical design standards. Additionally, ANSYS CFX, a numerical simulation program, was utilized. The number of disks and turbine capacity, as well as the link between inlet fluid pressure and turbine efficiency, were examined by the researchers. At 50 bar of pressure and a Reynolds number of 1.01×10^{1}, the prototype produced 76.52 watts of power. Computational fluid dynamics were used to effectively mimic the operation; the difference between the simulated and experimental results was no more than 9.3%. In terms of turbine rotor angular velocity, gas cooler and evaporator pressures, and the suggested heat pump cycle performance coefficient [17] examined the power production and available power loss of Tesla turbines. It has been demonstrated that a Tesla turbine cycle can outperform a traditional cycle with an expansion valve by up to 16.3%. Furthermore, the turbine power reaches its maximum at a rotor angular velocity of 1000 radians/s, thus increasing the inlet pressure raises the torque, which raises the turbine power. A thorough numerical analysis of Tesla's compact, bladeless turbine was given [18]. In this investigation, turbine efficiency as a function of the performance of various input nozzle apertures was demonstrated using computational fluid dynamics (CFD). Before investigating the impacts of various inlet nozzle apertures, a verification study was carried out utilizing the current manuscript. The findings demonstrate that the 4-inlet, four-hole (4i4o) configuration outperforms the 4-inlet, single-hole (4i1o) configuration in terms of speed and pressure distribution. Consequently, the torque value of the 4i4o configuration was 10% higher than that of the 4i1o version. When compared to earlier research, the performance of the Tesla turbine with the recommended ideal design has greatly improved.

Based on the findings of sensitivity analysis and the law of flow similarity [19] suggested a technique for downsizing Tesla turbines, including the stator and rotor. The disk outer diameter of a standard Tesla turbine, which was 100 mm, decreased to 50, 20, and 10 mm, respectively. Furthermore, a reduced single-channel turbine model and a multi-channel turbine model used in real-world applications have been developed by numerical simulation of Tesla's small turbines. The findings demonstrate the simplicity, rationality, and efficacy of the minimization technique that maintains the values of the two very significant dimensionless coefficients at their ideal levels. A single-channel Tesla turbine's isentropic efficiency marginally drops with decreasing size. Created a small-scale, effective Tesla turbine for isolated locations and conducted experimental research to evaluate it [20]. High torque cannot be produced by Tesla's turbine. A computer study and a pilot project to produce the turbine are included in this article. For 3D modeling, Solid Edge 2021 was utilized. Poly lactic acid (PLA) or ABS plastic are the materials utilized in the modeling. The 51 disks in the suggested design are spaced equally apart by 3 mm. This design produced an 81% rotation efficiency and a torque of 19.85 Nm. Because of the strong centrifugal force, it was discovered that the stress produced at the disks' edges was greater than at their core.

A Tesla turbine with 100 mm diameter disks, a central exhaust, and interchangeable nozzles were designed, manufactured [21]. Improved shape, nozzle position, and internal energy distribution have been made possible by computer-aided design models and computational fluid dynamics simulations, providing fresh perspectives on turbulence effects and viscous loss. The prototype reached a maximum efficiency of 8% when tested at pressures between 3 and 5 bars, which was in line with computational predictions. These findings demonstrate the promise of bladeless turbines in small-scale, low-pressure renewable energy applications. Suggested creating a tiny, incredibly effective Tesla turbine for isolated locations and testing it through experiments. For 3D modeling, Solid Edge 2021 was utilized [22]. Poly-lactic acid (PLA) or ABS plastic are the materials needed for modeling. The 51 disks in the suggested design are spaced equally apart by 3 mm. This design produced an 81% rotation efficiency and a torque of 19.85 Nm. It turns out that the strong centrifugal force causes more stress to be produced at the disks' edges than at their core. A new use for the Tesla turbine was introduced [23], who described it as a potential way to increase cooling cycle energy efficiency. The Redlich-K Wang equation of state defines methane as a genuine gas. To simulate computational fluid dynamics of heat and mass transfer using the finite volume approach, we employed complicated irregular network generation to create a low-deviation network in ANSYS Fluent. This study led to the proposal of useful design guidelines to help engineers find Tesla turbines that are optimum for predefined working circumstances, particularly in terms of power output, disk diameters, and rotational velocity.

Used Open FOAM software and computational fluid dynamics to examine the flow dynamics and energy loss of Tesla turbines [24]. The conversion of compressive energy into kinetic energy has been found to result in the largest loss, with estimates ranging from 64% to 88% of the total energy. At peak efficiency values, the amount of energy lost due to leakage between the rotor and the casing ranged from 4.97% to 7.95% of kinetic energy. Design changes, like the addition of a nozzle at the turbine inlet, can increase efficiency. Offered a thorough mechanical and technical analysis of Nikola Tesla's ground-breaking Tesla turbine [25]. The layout of bladeless axial disks installed on a central shaft and the fluid dynamic phenomena that produce torque across the viscous boundary layer between the disks are the main topics of the analysis, which focuses on the turbine's mechanical design. The work tackles efficiency and performance-related mechanical engineering

difficulties, emphasizing optimization strategies for disk number and spacing, nozzle engineering, and thermal management to lower the danger of overheating. Lastly, possible uses of micro-turbine technology for energy recovery and low enthalpy thermal cycles are examined. Inspired by Tesla's turbines [26] created a featherless turbine with a 250 mm diameter and a 0.5 mm air gap. Six distinct patterns were used to calculate the rotor dynamics characteristics of these turbines, and each pattern's critical speed was determined. Additionally, the finite element simulation approach was used to study flow field characteristics such air velocity and pressure. The turbine's highest rotational speed was 3200 rpm, and its maximum output torque was around 5.56 Nm at 992 rpm.

Carried out a study to evaluate a Tesla turbine's performance utilizing freely flowing water in a hose and water channel [27]. The performance of the turbine was observed at three different input position angles: tangential (0°, 30°, and 45° to water flow). At angles of 0°, 30°, and 45°, the power-efficiency relationship displayed a straight line. As the efficiency drops as the angle of the input location increases relative to the water flow increases, the results showed that angle 0° relative to the water flow is more efficient than angles 30° and 45°. A thorough review of the most recent advancements in Tesla disk turbine technology was provided [28], who concentrated on both theoretical modeling and experimental verification in a variety of energy applications. Complex viscosity-dominated flow dynamics within a rotor have been extensively studied using analytical frameworks and computational fluid dynamics simulations, emphasizing the impact of centrifugal forces, Coriolis, inertia, and viscosity on energy extraction. Disk geometry, disk spacing, and nozzle design all have a significant impact on performance; under ideal circumstances, isentropic flow efficiency exceeds 0.75. Overall, these initiatives validate the feasibility of Tesla turbines in applications where cost-effectiveness, scalability, and design flexibility are crucial, such as tidal energy extraction, organic Rankine cycles, small-scale cogeneration and heat systems, and small-scale renewable energy.

Research on Numerical Improvement of Tesla Turbine Efficiency, Rosen [29]. Inlet nozzle height, disk spacing, nozzle angle, pressure, and rotation speed were among the optimization criteria. Response surface approach was used for optimization. The compression ratio was disregarded as a neutral efficiency factor in the first step. The tangential velocity ratio, partial acceptance coefficient, degree of reaction, and dimensional ratio were found to be the most crucial factors required to attain optimal turbine efficiency in the second stage. Experiments confirmed that efficiency was nearly twice as good as the nominal model (from 9% to 17%). Computational fluid dynamics software was used to calculate the performance characteristics of the optimized turbine model. Critical elements include design flexibility, scalability, and ness. used data from an experimental campaign with R1233zd(E) as the working fluid to choose the reference state for computational analysis [30]. A 3D computer model was used to assess the fluid dynamics inside the stator, the gap between the stator and the rotor, and the rotor itself. The results of the 2D analytical program, which assumes uniform fluid entry into the rotor, agree with the performance outcomes of the 3D computational fluid dynamics.

A method that would improve the effectiveness of systems based on reverse cycles was examined [31]. Specifically, a Tesla turbine's two-phase flow behavior was investigated numerically. A newly created mathematical model and computational fluid dynamics analysis utilizing commercial software served as the foundation for two computational methods. The two-phase R404a fluid was calculated for a broad range of surface roughness, inter-plate gap size, and rotational speed. At a rotation speed of roughly 2000 rpm, the results demonstrate an average

output power of 0.8 W with a conductive torque of 3.6 m Nm. By modifying a suitable helix angle while preserving the average generated torque [32] suggested a method to smooth the torque produced by three-blade vertical axis wind turbines (3-PB). Using 3D numerical models, the aerodynamic characteristics of the turbine at various helix angles between 60° and 120°, along with the accompanying flow structures, were thoroughly examined at wind speeds of 7 m/s and terminal velocity ratios (TSRs) between 0.44 and 1.77. The findings indicate that an 80° helical angle yields the optimum results. With nearly total stability in the average torque coefficient, a notable reduction in the turbine torque coefficient's departure from its average was noted.

2. Geometrical and mathematical model of Curved -Plate Drag Turbine

By transforming the kinetic energy of a pressured air stream into mechanical rotational energy, the proposed Curved-plate drag turbine is intended to recover otherwise squandered pneumatic energy. The turbine is made up of many Curved plates that are housed in a flow-guiding enclosure and rotated on a shaft. Aerodynamic drag forces are produced when waste air is injected through the intake and directed toward the plate surfaces. The shaft rotates as a result of the torque created by the resulting forces on the rotor. To create electrical energy, the mechanical power is then transmitted to an electrical generator. Under regulated waste-air operating circumstances, the experimental study aims to assess the impact of electrical loading on turbine rotational speed, produced voltage, current, and output power. The outer shell, also known as the main housing, guarantees accurate fluid flow control, protects internal components, and strengthens structural integrity. The main organ in charge of transmitting kinetic energy from the air to the axis is the curved-plate drag turbine. The central axis that transfers mechanical motion to the external load is the rotating shaft, also known as the drive shaft. Inlet port: To rotate the disks, the compressed fluid (liquid or Air) is introduced tangentially. After the fluid has lost most of its kinetic energy in the spiral path toward the center, it can depart through the exit port, also known as the outlet port. The mechanical stability required to put the turbine on a variety of platforms and constructions is provided by the mounting base.

The primary design and geometrical specifications of the suggested Curved-Plate Drag Turbine model are shown in Table 1. The size of the curved plates, rotor geometry, plate spacing, shaft diameters, and other pertinent construction factors are among the elements that characterize the turbine configuration. These dimensions were chosen to allow the aerodynamic drag force to be transformed into rotating mechanical energy by creating an appropriate contact between the curved plates and the entering wasted compressed-air stream. The given parameters guaranty repeatability of the experimental testing under various air-pressure and electrical-load situations and offer a consistent basis for producing the experimental model.

Table 1: Curved -Plate Drag Turbine model parameters

Symbol	Description	Symbol	Description
T	Torque, N.m	Q	Water discharge, m3/s
F	Force, N.	A	Cross-sectional area of the water source, m2
A_p	Projected area of one plate (m^2)	Cd	Discharge coefficient = 0.60
V	Velocity with respect to the moving plate (m/s)	L	Weir width, m.

L	Length of the lever arm, m.	h	Water overflow head, m.
T	Torque, N.m	Vol	Known volume of container
N	Shaft rotating speed, rpm	t	Time to fill the container with a known volume, sec.
P_h	Hydropower, W.	δ	Density of water, 1000 kg/m^3
Q_t	Volumetric flow rate, m^3/s	F_D	Aerodynamic drag force (N)
H	Head of water, m.	ρ	Air density (kg/m^3)
g	Gravitational acceleration, 9.81 m/s^2	C_D	Drag coefficient of the curved plate

2.1 Speed of Curved -Plate Drag Turbine

A tachometer was used to gag the curved -Plate Drag Turbine speed. The device's sensor is inserted into the rotating shaft to measure the number of revolutions per minute to get speed data. For ten continuous minutes, the data was recorded every minute.

2.2 Torque of Curved -Plate Drag Turbine

A brake torque meter was used to track the torque produced by Tesla's turbine. The following formula was used to determine Tesla's turbine torque [27]:

$$F_D = \frac{1}{2}\,\rho\, C_D\, A_p V^2 \qquad (1)$$

2.3 Water flow rate (Q) and height difference (head)

The formula for the volume approach of determining water discharge is shown in equations (2) and (3). The volume of liquid flowing across a given cross-sectional area in each amount of time is known as the flow rate of water or another liquid (Q).

The water flow rate has been calculated using a variety of techniques. Weir's formula, which determines how long it takes to fill a container of a specific size, is one of the techniques examined in this study. This technique is sometimes referred to as the volume method or the bucket method. In both the centrifugal pump experiment and the dam channel experiment, the water flow rate steadied during the observations. Equation (2) was used to compute the water flow along the rectangular dam, while the centrifugal pump was used to obtain the water flow rate using the bucket method and Equation (3).

$$Q = \frac{2}{3} C_d L \sqrt{2gh^{1.5}} \quad ,\left(\frac{m^3}{s}\right) \qquad (2)$$

$$Q = \frac{V_{ol}}{t} \quad ,\left(\frac{m^3}{s}\right) \qquad (3)$$

2.4 Measurement of power

The torque of a machine shaft is measured using a dynamometer. Equation (4) was used to compute mechanical power and measure torque around the rotating shaft. A tachometer was used to examine and quantify the machine's rotational speed (N).

$$P = 2\pi \mathrm{TN} \qquad (4)$$

Hydroelectric power is the energy produced by using an elevation difference to extract potential energy from water. Energy from water, or hydropower, can be transformed into mechanical energy and put to immediate use, when a generator is used to transform it into electrical energy. Equation (5) was used to compute this hydroelectric power, which can be extracted from water and is directly proportional to the flow height and flow rate.

$$P_h = Q_t H \delta g \qquad (5)$$

2.5 Curved -Plate Drag Turbine efficiency

To determine the efficiency of a Curved -Plate Drag turbine, equation was used.

Entropy is an irreversible energy conversion process. The formula for a fluid's kinetic energy transfer is as follows if the effects of heat transmission are disregarded:

$$\rho \frac{DE}{Dt} = \rho f . u + (\nabla . u)\rho + \nabla . (S_T . u) - \varphi \qquad (6)$$

where S_T is the stress tensor: $S_T = 2\mu S_r - (p + \frac{2}{3\mu(\nabla . u)}$ I. Sr, I and m are the strain rate tensor, unit tensor and dynamic viscosity, respectively. The u is the relative velocity; r is the density of fluid.

φ The fluid's viscous dissipation function with $\varphi = -\frac{2\mu(\nabla . u)^2}{3} + 2\mu S_r$.

Water behaves like an incompressible liquid when the cavitation event is ignored. Tensor decomposition law allows for the expression of φ as:

$$\varphi = \mu|\varpi|^2 \text{ -2 } \mu\nabla . ((\nabla . u)I - \nabla u^T . u \qquad (7)$$

$$\rho \frac{DE}{Dt} = -\nabla . (\rho u) - \nabla . (u\varpi \times u) - \mu|\varpi|^2 \qquad (8)$$

where vorticity is represented by ϖ. The unit work from the surface pressure gradient in the streamline direction is the first term on the right side of the equal sign; the nonlinear effects of vorticity and velocity field in viscous fluids are the second term; and the energy loss due to viscosity and turbulent fluctuations is the final term. $W = \mu|\varpi|^2$is the rate at which entropy is generated, which is always positive and closely correlated with energy loss?

The entropy generation rate function for an incompressible flow can be expressed as follows:

$$W = \mu\left[(\frac{\partial w}{\partial y} - \frac{\partial v}{\partial z})^2 + (\frac{\partial u}{\partial z} - \frac{\partial w}{\partial x})^2 + (\frac{\partial v}{\partial x} - \frac{\partial u}{\partial y})^2\right] \quad (9)$$

In contrast, the entropy generation rate for turbulent flow may be divided into two terms following the Reynolds time averaged process: the turbulent entropy generation rate (W_{vis}) and the viscous entropy generation rate (W_{tur}).

$$W = W_{vis} + W_{tur} \qquad (10)$$

$$W_{vis} = \mu\left[(\frac{\partial \overline{w}}{\partial y} - \frac{\partial \overline{v}}{\partial z})^2 + (\frac{\partial \overline{u}}{\partial z} - \frac{\partial \overline{w}}{\partial x})^2 + (\frac{\partial \overline{v}}{\partial x} - \frac{\partial \overline{u}}{\partial y})^2\right] \quad (11)$$

$$W_{tur} = \mu\left[\overline{(\frac{\partial w}{\partial y} - \frac{\partial v}{\partial z})^2} + \overline{(\frac{\partial u}{\partial z} - \frac{\partial w}{\partial x})^2} + \overline{(\frac{\partial v}{\partial x} - \frac{\partial u}{\partial y})^2}\right] \quad (12)$$

The velocity field can be used to determine W_{vis}s once the RANS equation has been solved. Nonetheless, it is not directly from simulation simulation outcomes. According to Kock et al. [35], the loss resulting from turbulence (also known as turbulent loss) is directly associated with the turbulence model employed in the computations; hence, W_{tur} is defined It is the result of multiplying the fluid's density by the turbulent vortex' dissipation rate (ε).

$$W_{tur} = \rho\epsilon \tag{13}$$

There is a large energy loss due to the velocity gradient in the wall entropy generation rate [36,37] (W_{wall}) can be computed by

$$W_{wall} = \sigma.u \tag{14}$$

$$P_{vis} = \int_0^v W_{vis}\, dv \tag{15}$$

$$P_{tur} = \int_0^v W_{tur}\, dv \tag{16}$$

$$P_{wall} = \int_0^s W_{wall}\, ds \tag{17}$$

$$P_{egr} = P_{vis} + P_{tur} + P_{wall} = P_{vol} + P_{wall} \tag{18}$$

The following formulas were used to compute the hydraulic height, shaft capacity, and efficiency of a pump-driven turbine (PAT) under various flow conditions.

$$H = \frac{P_{in} - P_{out}}{\rho g} \tag{19}$$

$$P = M.\frac{2\pi n}{60} \tag{20}$$

$$\eta = \frac{P}{\rho g Q H} \tag{21}$$

$$\frac{\partial}{\partial x_i}(\rho\overline{u_i}) = 0 \tag{22}$$

$$\frac{\partial}{\partial x_j}\left(\rho\overline{u_i u_j}\right) = \frac{\partial\overline{\rho}}{\partial x_i} + \frac{\partial}{\partial x_j}\left[\mu\left(\frac{\partial\overline{u_i}}{\partial x_j} + \frac{\partial\overline{u_j}}{\partial x_i} - \frac{2}{3}\delta_{ij}\frac{\partial\overline{u_k}}{\partial x_k}\right)\right] + \frac{\partial}{\partial x_j}\left(-\rho\acute{u}_i u_j\right) \tag{23}$$

$$\frac{\partial(\rho k)}{\partial t} + \frac{\partial(\rho\overline{u}_j)}{\partial x_j} = \tilde{P}_k - \beta^*\rho k\omega + \frac{\partial}{\partial x_j}\left[\left(\mu + \frac{\mu_t}{\sigma_{k3}}\right)\frac{\partial k}{\partial x_j}\right] \tag{24}$$

$$\frac{\partial(\rho\omega)}{\partial t} + \frac{\partial(\rho\overline{u}_j\omega)}{\partial x_j} = \frac{\partial}{\partial x_j}\left(\left(\mu + \frac{\mu_t}{\sigma_{\omega 3}}\right)\frac{\partial\omega}{\partial x_j}\right) + \alpha_3\frac{\omega}{k}\tilde{P}_k - \beta_3\rho\omega^2 + (1 - F_1)2\rho\frac{1}{\omega\sigma_{\omega 2}}\frac{\partial k}{\partial x_j}\frac{\partial\omega}{\partial x_j} \tag{25}$$

$$\mu_t = \frac{\rho a_1 k}{\max(a_1\omega, SF_2} \tag{26}$$

$$\overline{X} = \frac{\sum X_m}{z} \tag{27}$$

$$SD = \sqrt{\frac{\sum_{m=1}^{z}(x_m - \overline{X})^2}{z-1}} \quad (28)$$

$$U = \frac{SD}{\sqrt{z}} \times 100\% \quad (29)$$

$$\nabla\eta_{abs} = |\eta_{EXP} - \eta_{CFD}| \quad (30)$$

$$\nabla\eta_{rel} = \frac{\nabla\eta_{abs}}{max\{\eta_{EXP}, \eta_{CFD}\}} \times 100\% \quad (31)$$

3. Design of the Curved-Plate Drag Turbine in AutoCAD

Using AutoCAD, an accurate two-dimensional and three-dimensional representation of the suggested turbine shape was created for the curved-plate drag turbine as shown in figure 2. A central spinning shaft is attached to a number of curved plates that are evenly spaced around the turbine's circle. As drag surfaces, the curved plates absorb the momentum of the incoming wasted air pressure and transform it into mechanical energy that rotates. Each plate's curve and position were chosen to maximize the effective aerodynamic drag force while permitting smooth airflow around the turbine. The AutoCAD model was used to determine the primary geometric characteristics, such as the plate length, breadth, thickness, curvature radius, number of plates, shaft diameter, and turbine outer diameter. Stable rotation and balanced mass distribution were ensured by maintaining precise angular separation between the plates. The finished CAD model enables the investigation of the impact of turbine shape on rotational speed, torque, and electrical power output in addition to providing the dimensional reference needed for manufacturing and experimental testing.

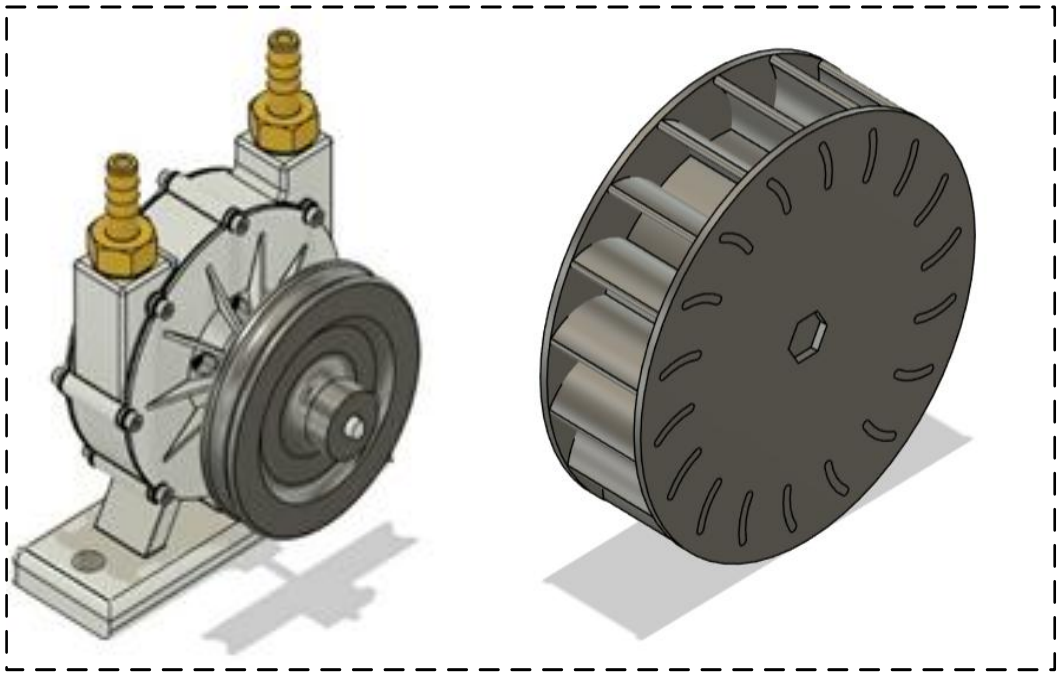

Figure 2. Design of the Curved-Plate Drag Turbine in AutoCAD

3.1 Dimensions of the proposed model

The dimensions and geometric layout of the suggested Curved-Plate Drag Turbine model are shown in Figure 3. The rotor diameter, shaft dimensions, curved plate dimensions, plate curvature, space between the plates, and overall turbine design are all depicted in the picture. These proportions were chosen such that the curved plates and the incoming wasted air pressure would interact appropriately, creating aerodynamic drag and rotor motion. The purpose of the curved-plate design is to efficiently catch the air stream and transform a portion of its pneumatic energy into mechanical rotational energy. Additionally, a constant and repeatable turbine shape for the experimental study is backed up by the specified specifications. The dimensional model serves as the foundation for construction and enables an experimental assessment of the effects of applied air pressure and electrical loading conditions on the turbine's rotational speed and electrical power output.

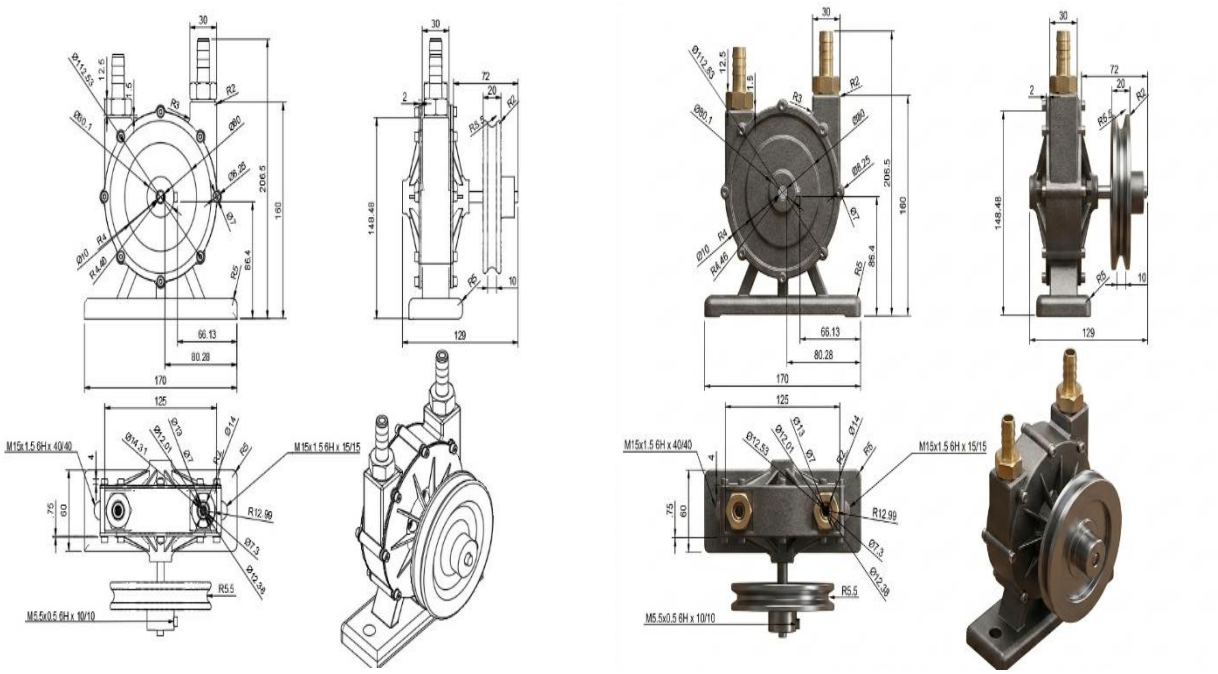

Figure 3. The Dimensions of the proposed Curved-Plate Drag Turbine model.

3.2 Realistic Production of the Curved-Plate Drag Turbine

CNC machining and 3D printing were used in the practical fabrication of the suggested Curved-Plate Drag Turbine. Based on the dimensions and geometry created in the AutoCAD design, a CNC machine was used to build the turbine cover and related structural elements as shown in figure 4. In order to achieve exact circular alignment, correct dimensions, and a clean interior surface for the turbine housing, CNC machining was used. Using a 3D printer, the curved turbine plates were produced straight from the three-dimensional CAD model. This method made it possible to precisely and reliably replicate the necessary curvature, thickness, and angular arrangement of the plates. Following manufacturing, the central shaft was installed on appropriate bearings within the CNC-machined cover after the curved plates were joined around it with consistent angular spacing. The mechanical rotation created by the wasted air pressure was then converted into electrical power by connecting the turbine assembly to an electrical generator. CNC machining and 3D printing together provide a useful and economical way to produce the prototype while preserving the geometric precision needed for exploratory research.

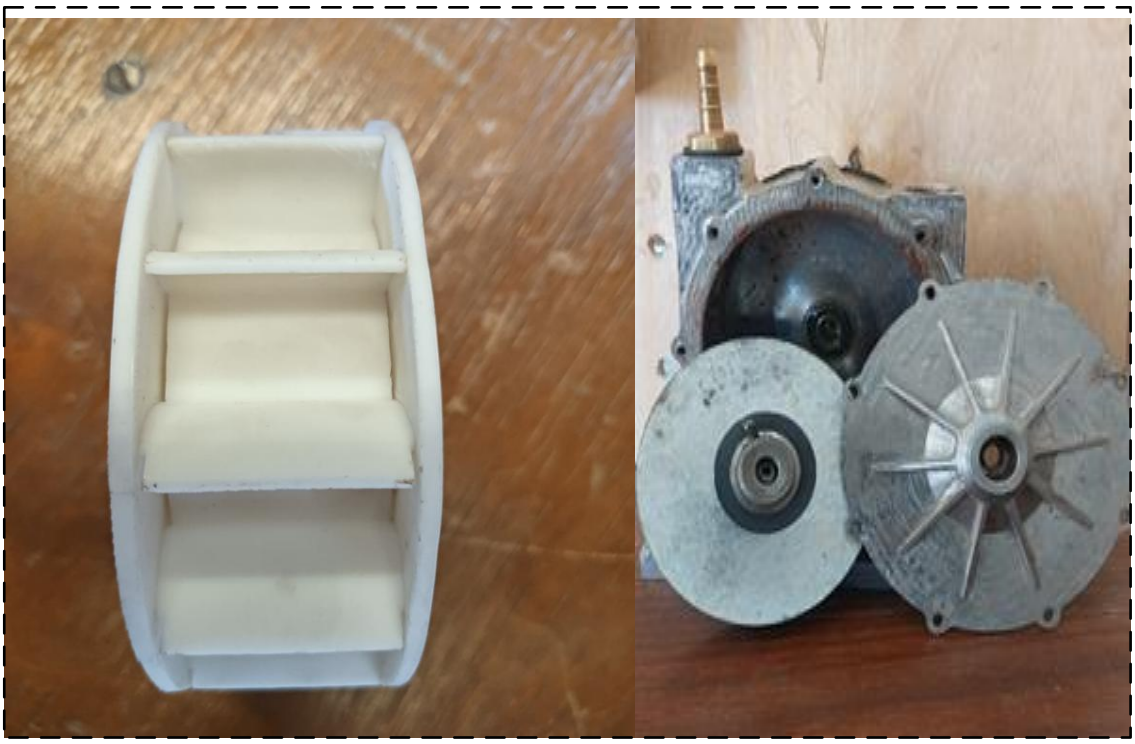

Figure 4. Production of the Curved-Plate Drag Turbine in CNC machining and 3D printing

3.1 Test Rig for Experimental

The two projections of the experimental test rig created to examine the performance of the suggested Curved-Plate Drag Turbine under various operating and electrical loading circumstances are shown in Figure 5. The main parts of the test rig are as follows: (1) compressor, which provides the turbine with controlled airflow, (2) pressure gage, which measures the air pressure supplied to the system, and (3) electrical generator, which is mechanically connected to the turbine to transform the rotational energy produced into electrical power. (4) a pulley-equipped Curved-Plate Drag Turbine, (5) a belt and pulley gearbox that delivers mechanical power from the turbine shaft to the generator, (6) RPM, current, and voltage sensors were installed on the experimental test rig to gage the Curved-Plate Drag Turbine's mechanical and electrical performance. To determine the rotating speed in revolutions per minute (rpm), an RPM sensor was installed on the turbine shaft. While the voltage sensor monitored the generator terminal voltage, the current sensor was attached to the generator output circuit to measure the electrical current supplied to the applied load, (7) computer to monitor, record, and analyze the experimental measurements, (8) electrical load to apply various loading conditions to the generator, and (9) data-acquisition system to gather the measured mechanical and electrical parameters. Because of the way these parts are arranged, the turbine may be tested under regulated air pressure and electrical load circumstances, allowing for the experimental evaluation of the effects of operating pressure and generator load on rotational speed, voltage, current, and produced power.

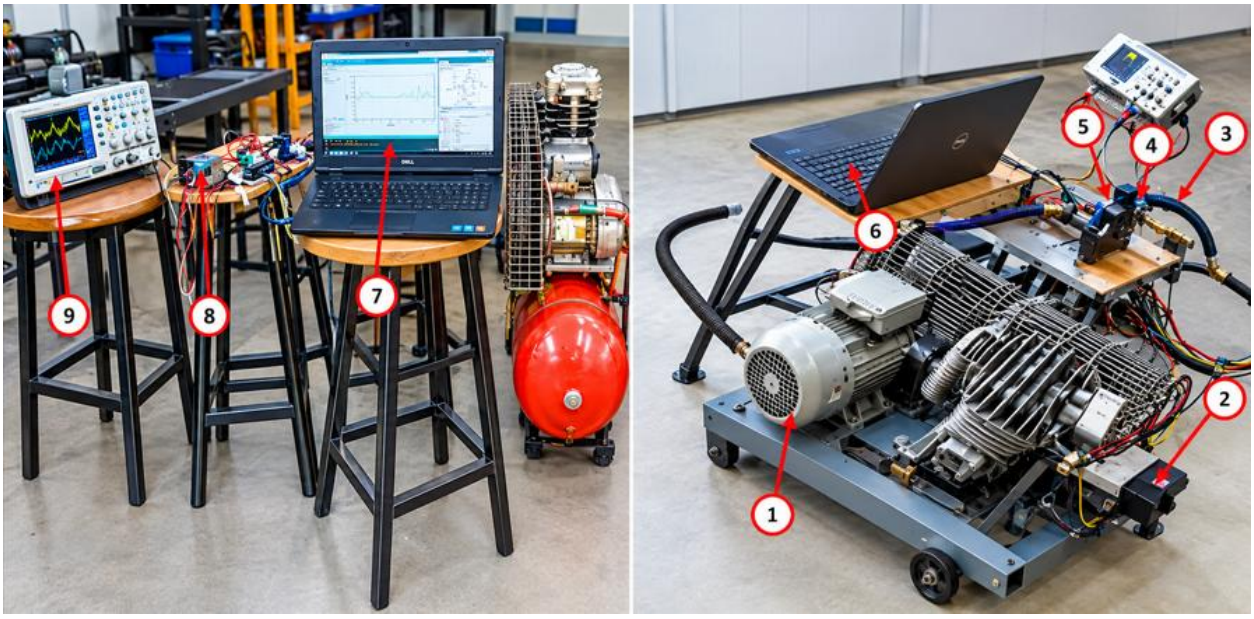

1- Compressor 2- Pressure gauge 3- Generator 4-Curved-Plate Drag Turbine with pulley 5- Belt pulley 6- RPM, current, and voltage sensor 7-computer 8- Load 9- Data acquisition.

Figure 5. The two projections of the test rig

4. The Result and Discussion

The compressor was first charged to a maximum pressure of 120 LB/in² (120 psi) during the experimental testing. The pressure supplied to the Curved-Plate Drag Turbine was continually monitored using the pressure gage. The related turbine performance characteristics were recorded as the pressure steadily dropped from 120 to 90 LB/in² (psi) during the testing. It was also determined how long it took for the pressure to drop from 120 to 90 psi. In order to assess the impact of lowering pressure on turbine rotational speed, generator voltage, current, and electrical power generation, this process offered a controlled range of air-pressure conditions.

To precisely gage the Curved-Plate Drag Turbine's performance, an RPM, voltage, and current sensor were installed in the experimental test rig. The turbine rotational speed in revolutions per minute (rpm) was continually measured by the RPM sensor, which was mounted on the revolving shaft. While the current sensor monitored the electrical current delivered to the connected load, the voltage sensor was attached to the electrical generator output to measure the generated terminal voltage. The data-acquisition system received the measured signals, which were then recorded on a computer for further examination. The observed voltage and current were used to compute the electrical power produced by the turbine-generator system using (P=VI). The effects of air pressure and electrical load on turbine speed and electrical power output were assessed using these data.

4.1 Data by Sensors Lab Acquisition

The Curved-Plate Drag Turbine's rotational speed fluctuation under four distinct electrical loading scenarios is shown in Figure 6. A 3 Ω resistive load is used in the first load instance, whereas 5 Ω and 7 Ω resistive loads are used in the second and third load cases, respectively. A DC motor load coupled to the generator is depicted in the fourth scenario. For every load scenario, the turbine speed was measured while keeping the experimental air-pressure range constant. The graphic shows how the electrical load affects the turbine-generator system's rotating speed.

Turbine rotational speed varies in proportion to changes in electrical loads because the generator needs a different electromagnetic torque. An experimental evaluation of the Curved-Plate Drag Turbine's capacity to sustain rotational performance under various generator loading circumstances is provided by comparing the four scenarios.

As the compressor pressure dropped from 120 to 90 LB/in² (psi), Figure 7 compares the voltage produced by the Curved-Plate Drag Turbine under four distinct electrical loading scenarios. A 3 Ω resistive load was used in the first load instance, a 5 Ω resistive load in the second, a 7 Ω resistive load in the third, and a DC motor as the electrical load in the fourth. Throughout the pressure decrease, the voltage sensor was used to continually monitor the voltage produced by the turbine-generator system. The findings show how the produced voltage is affected by both the applied electrical load and the dropping air pressure. Generally speaking, variations in electrical loading modify the generator's operating point, which in turn affects the terminal voltage; conversely, a decrease in compressor pressure causes a corresponding change in the mechanical energy that is available and the speed at which the turbine rotates. An experimental assessment of the Curved-Plate Drag Turbine's voltage-generation capacity across the pressure range of 120–90 psi is provided by the comparison of the four load scenarios.

As the compressor pressure dropped from 120 to 90 LB/in² (psi), Figure 8 compares the electrical current produced by the Curved-Plate Drag Turbine under four distinct electrical loading scenarios. Three Ω resistive loads were utilized in the first load instance, five Ω resistive loads were used in the second, seven Ω resistive loads were used in the third, and a DC motor was used as the electrical load in the fourth. Throughout the pressure drop, the generator output current was continually measured using the current sensor. The graphic shows how the available air pressure and the electrical load affect the produced current. While the DC motor offers a dynamic electrical and mechanical load that may result in a distinct current response, the current for resistive loads changes according to the generator voltage and the matching load resistance. The generator current varies in proportion to changes in the available pneumatic energy and turbine operating speed when the compressor pressure drops from 120 to 90 psi. An experimental evaluation of the current-generation Curved-Plate Drag Turbine's performance under various loading scenarios is provided by comparing the four scenarios.

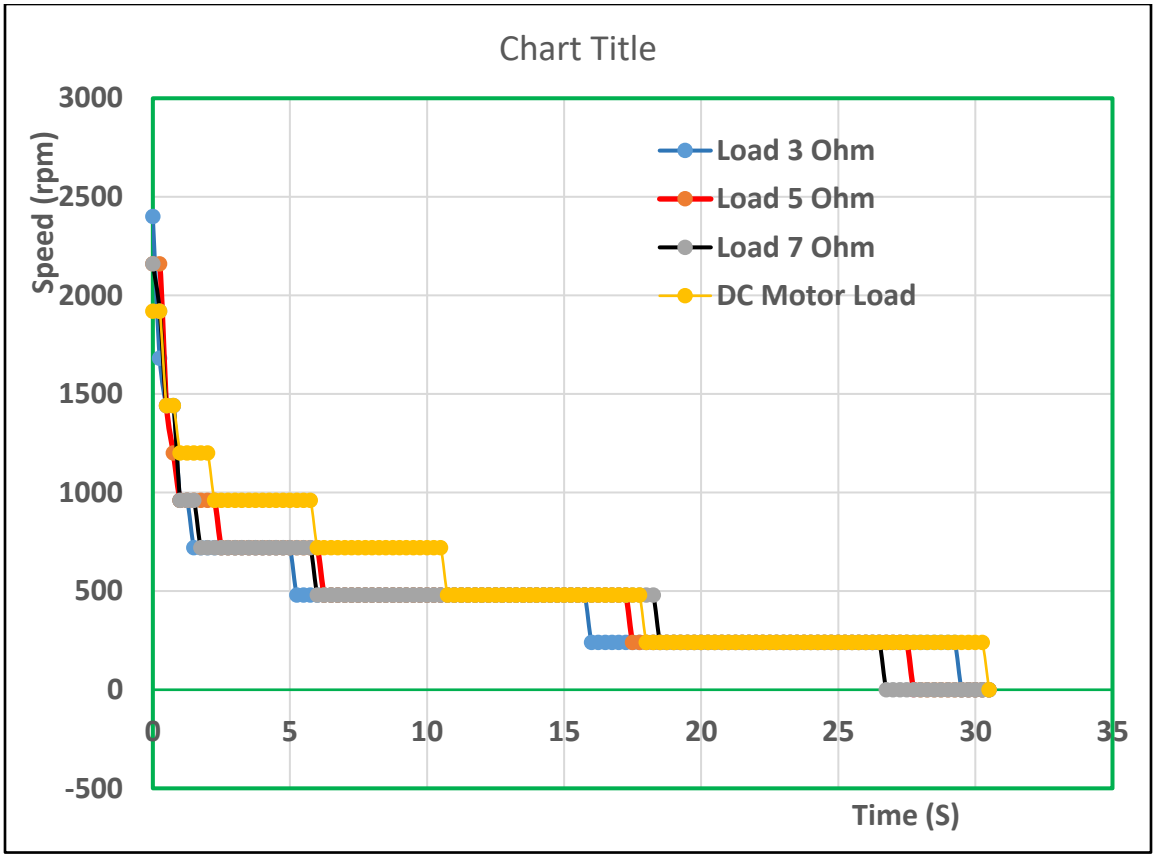

Figure 6. The speed comparison between the four load cases

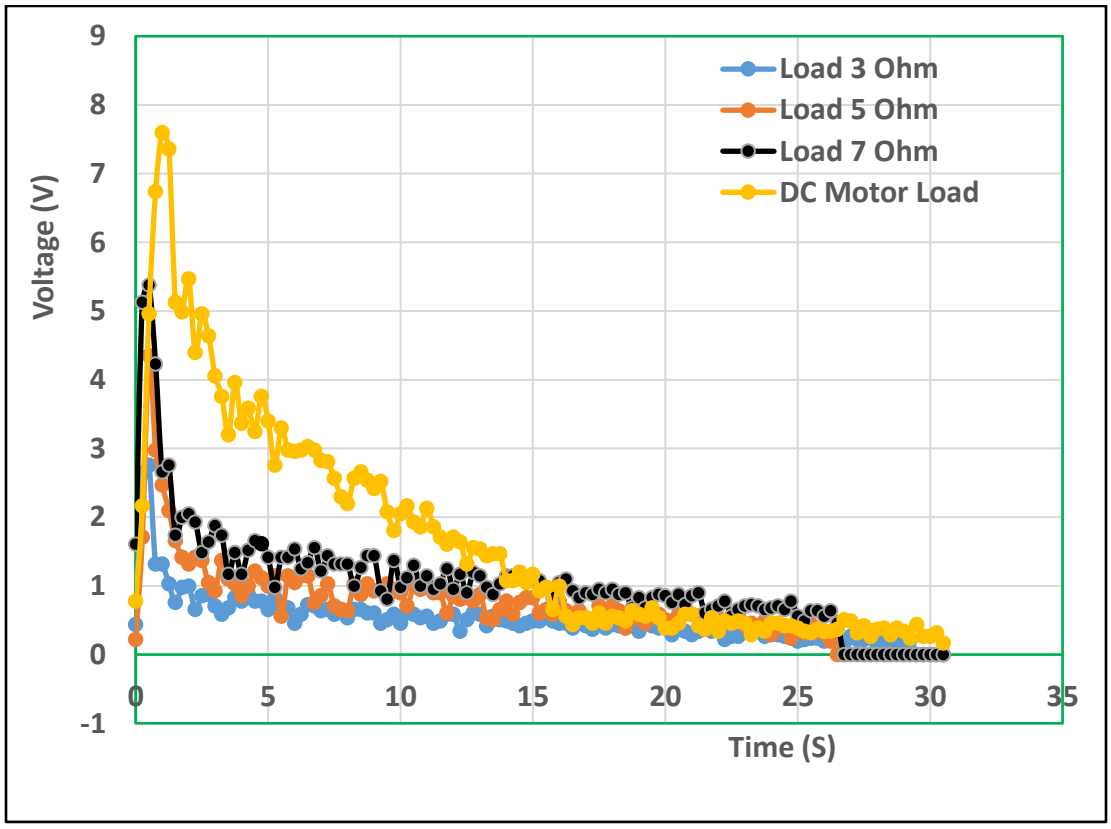

Figure 7. The voltage comparison between the four load cases

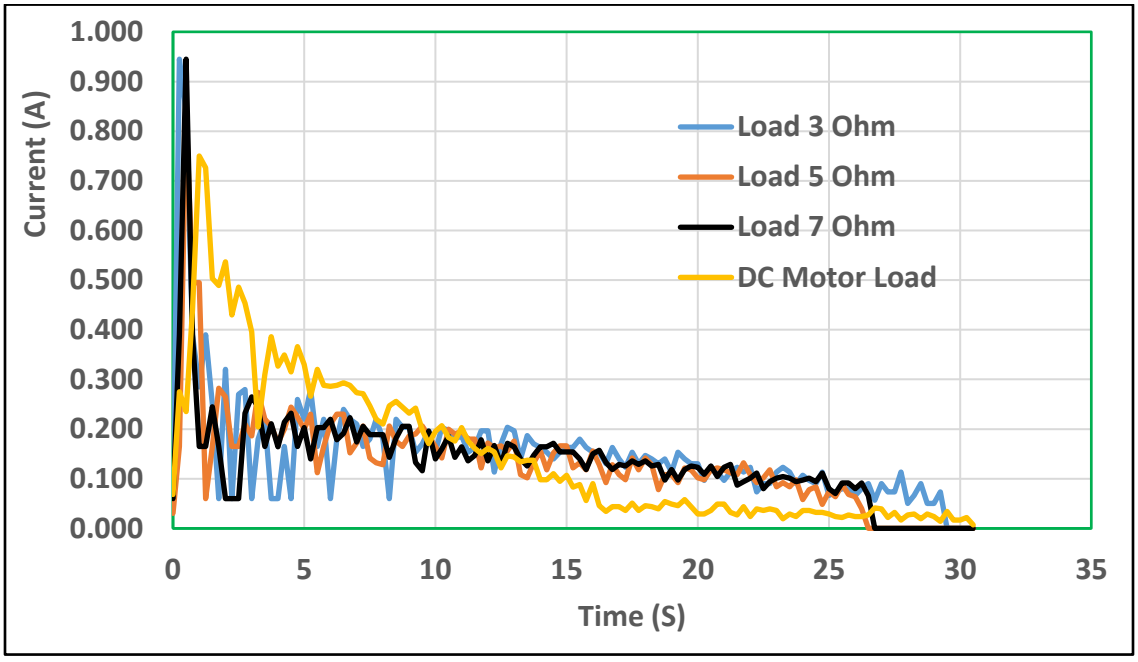

Figure 8. The current comparison between the four load cases

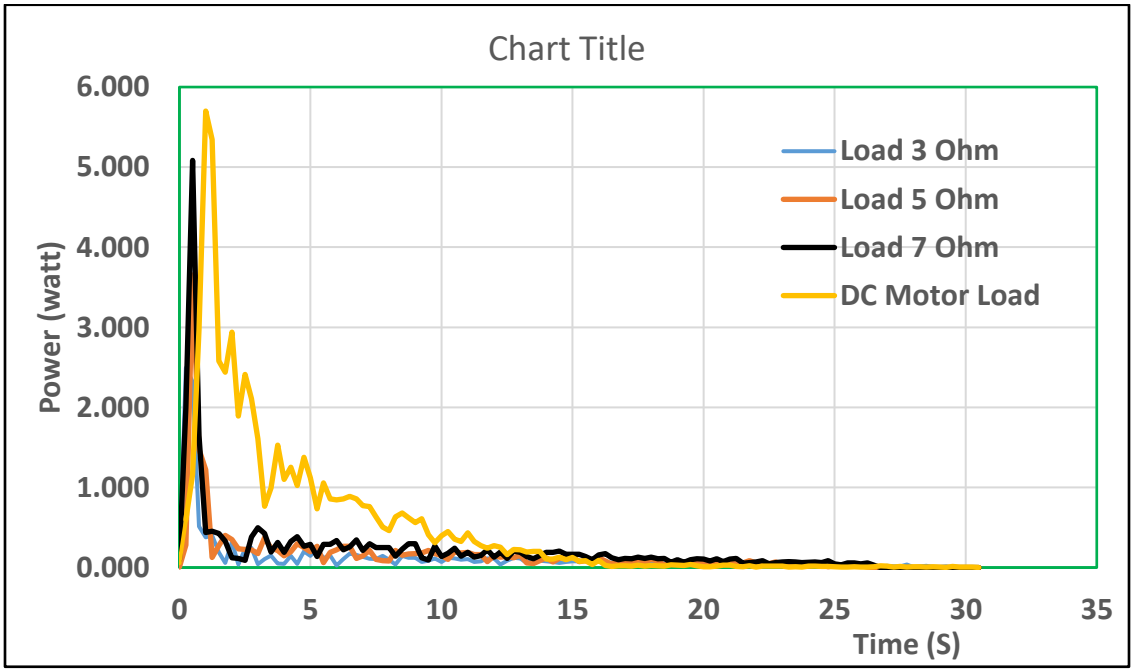

Figure 9. The power comparison between the four load cases

The Curved-Plate Drag Turbine's electrical power output under four distinct electrical loading scenarios is compared in Figure 9 as the compressor pressure dropped from 120 to 90 LB/in² (psi). A 3 Ω resistive load was used in the first load instance, a 5 Ω resistive load in the second, a 7 Ω

resistive load in the third, and a DC motor as the electrical load in the fourth. Using (P=VI), the produced electrical power was calculated from the observed voltage and current. The graphic shows how the turbine-generator system's power production is affected by both the electrical demand and the dropping air pressure. The available pneumatic energy provided to the turbine varies as the compressor pressure drops, which has an impact on the turbine's rotational speed and, ultimately, the generator power output. Furthermore, the generator is subjected to varying electrical and mechanical working circumstances due to the various loads, which results in variable power responses for each scenario. An experimental assessment of the Curved-Plate Drag Turbine's power-generating capacity across the pressure range of 120–90 psi is provided by comparing the four load scenarios.

4.2 Data by Oscilloscope

The Curved-Plate Drag Turbine's voltage comparison under four distinct electrical load scenarios is shown in Figure 10 and Figure 11 as the compressor pressure dropped from 120 to 90 LB/in² (psi). A 3 Ω resistive load was used in the first test, a 5 Ω resistive load in the second, a 7 Ω resistive load in the third, and a DC motor load in the fourth. An oscilloscope was used to measure the generator output voltage at various points throughout the pressure decrease. The oscilloscope was set up with a voltage scale of 2 V/div, which means that each vertical division represents 2 V, and a time scale of 5 s/div, which means that each horizontal division represents 5 s. These configurations made it possible to clearly see the produced voltage waveform's magnitude and temporal fluctuation for every load state. The recorded waveforms show how the electrical loading state affects the generator output and how the produced voltage varies over time as the available air pressure drops. The voltage response and stability of the Curved-Plate Drag Turbine under various electrical loads may be directly evaluated experimentally by comparing the four scenarios.

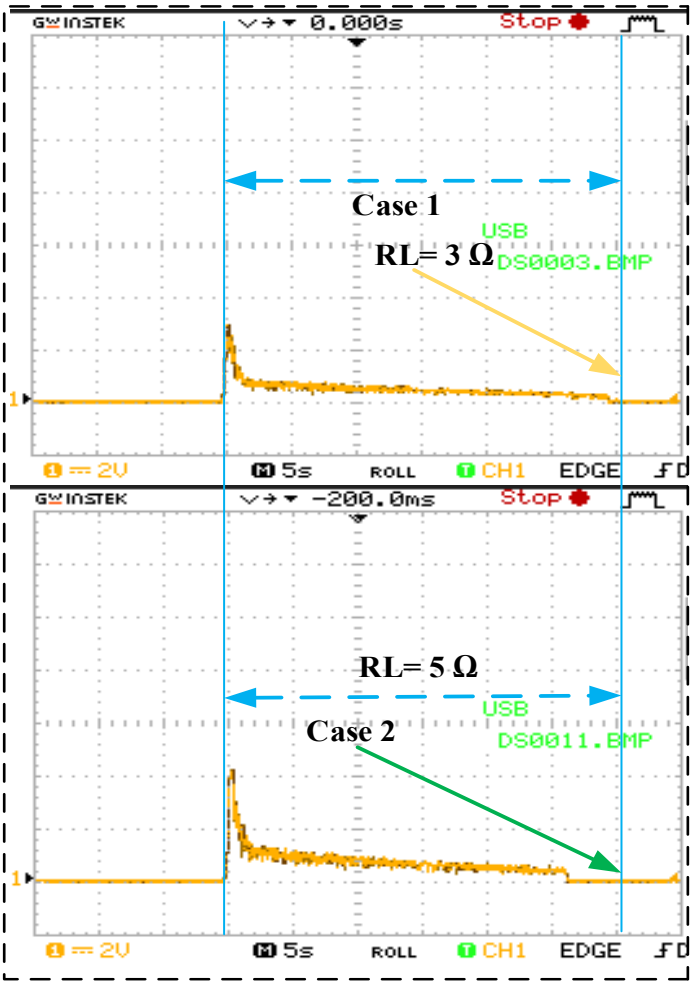

Figure 10. Curved-Plate Drag Turbine's voltage comparison under 3 ohms, and 5-ohm distinct electrical load scenarios

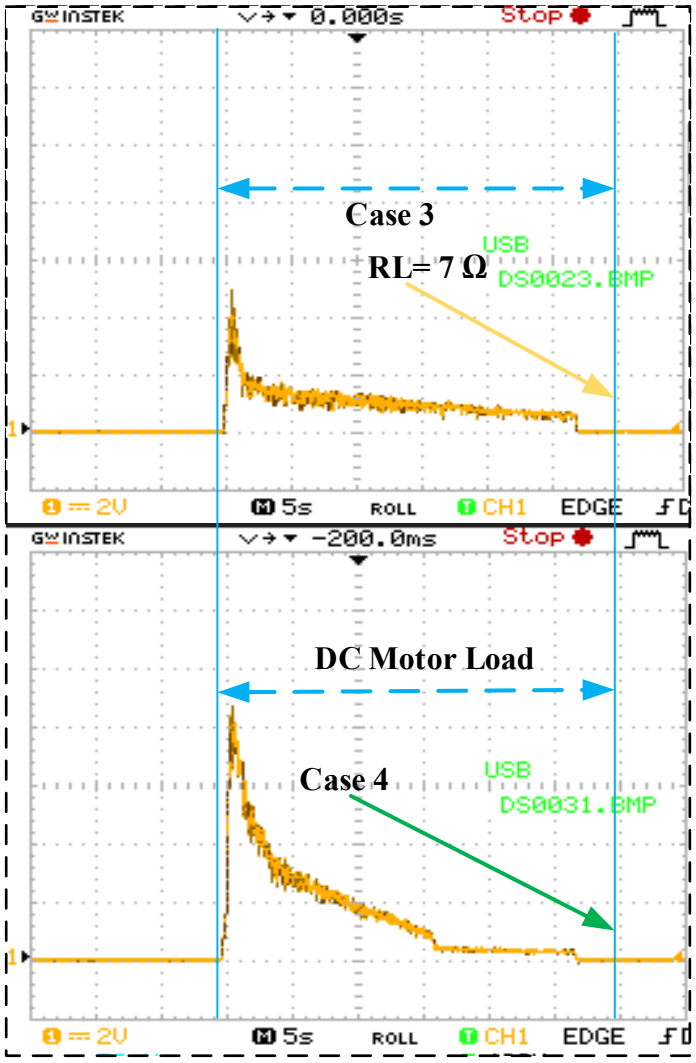

Figure 11. Curved-Plate Drag Turbine's voltage comparison under 7 ohms, and DC Motor distinct electrical load scenarios

4.3 Comparison for Change Load

The effect of varying the electrical load at 3-second intervals on the suggested system's performance is shown by comparing the four load scenarios as illustrated in table 2. The average voltage, current, rotational speed, and power in Change Load Case 1 were, respectively, 1.18 V, 0.32 A, 1015.38 rpm, and 0.56 W. In Case 2, the average voltage rose to 1.77 V, the average speed climbed to 1033.85 rpm, the average current dropped to 0.27 A, and the average power was 0.66 W when the load state was altered. In Case 3, the produced power climbed to 0.90 W, the average speed stayed about 1033.85 rpm, and the voltage further increased to 2.65 V while the current dropped to 0.25 A. With an average voltage of 4.87 V, a current of 0.45 A, and a rotating speed of 1200 rpm, Case 4 ultimately generated the highest recorded values, yielding the greatest average power of 2.45 W. Overall, the findings show that the electrical load situation has a major impact on the system's observed voltage, current, rotating speed, and power production. The final load condition delivered much greater electrical output under the measured operating circumstances, as seen by the rise in average power from 0.56 W in Case 1 to 2.45 W in Case 4.

Table 2: Comparison between four cases at change load through 3 second

Change Load	Average Power (W)	Average Speed (rpm)	Average Ampere (A)	Average Voltage (V)
Change Load Case 1	0.56	1015.38	0.32	1.18
Change Load Case 2	0.66	1033.85	0.27	1.77
Change Load Case 3	0.90	1033.85	0.25	2.65
Change Load Case 4	2.45	1200.00	0.45	4.87

The average produced voltage for each of the four changing-load scenarios is compared in Figure 12, where the electrical load is varied every three seconds. In Cases 2, 3, and 4, the average voltage rose gradually from 1.18 V in Change Load Case 1 to 1.77 V, 2.65 V, and 4.87 V, respectively. This translates to a total increase of around 312.7% between Cases 1 and 4. The findings show that depending on the applied load state, the generator voltage changed considerably. Case 4 had the greatest average voltage of 4.87 V and the highest observed rotating speed of 1200 rpm. These findings show that the produced voltage was significantly impacted by the fluctuating electrical demand and the generator's associated operating parameters.

The average voltage produced under four distinct changing-load scenarios in which the electrical load was switched every three seconds as shown in the figure 12. The average voltage clearly rises as the load scenario goes on, according to the data.

- Change Load Case 1: 1.18 V was the average voltage.
- Change Load Case 2: Compared to Case 1, the average voltage rose to 1.77 V, or around 50%.
- Change Load Case 3: Compared to Case 1, the average voltage rose by an additional 124.6%, reaching 2.65 V.
- Change Load Case 4: At 4.87 V, the greatest average voltage was measured, which is almost 312.7% greater than Case 1.

The steadily rising voltage shows that the experiment's shifting load circumstances had a significant impact on the generator output voltage. Case 4 yielded the greatest voltage and the highest observed rotational speed (1200 rpm). This implies that a greater electrical potential at the generator terminals was caused by the operating conditions related to Case 4.

The average current under four distinct changing-load scenarios is compared in Figure 13, where the electrical load is adjusted every three seconds. The average current dropped to 0.27 A and 0.25 A in Cases 2 and 3, respectively, from 0.32 A in Change Load Case 1. On the other hand, Case 4 produced a discernible rise in the average current to 0.45 A, the highest figure of the four situations studied. The change in current shows that the generator's operating state and the shifting load had an impact on the electrical current response. In contrast to the preceding three load instances, Case 4's maximum current was recorded at the same time as its greatest reported rotational speed of 1200 rpm. Overall, the experimental findings show that the generator current responsiveness varied measurably when the electrical load was changed every three seconds.

- In Case 1 of Change Load, the average current was 0.32 A.
- Change Load Case 2: Compared to Case 1, the average current dropped to 0.27 A, a decrease of almost 15.6%.

- Change Load Case 3: In comparison to Case 1, the current dropped by around 21.9% to 0.25 A, a modest additional decrease.
- Change Load Case 4: The average current rose dramatically to 0.45 A, the greatest current of the four examples and around 40.6% higher than Case 1.

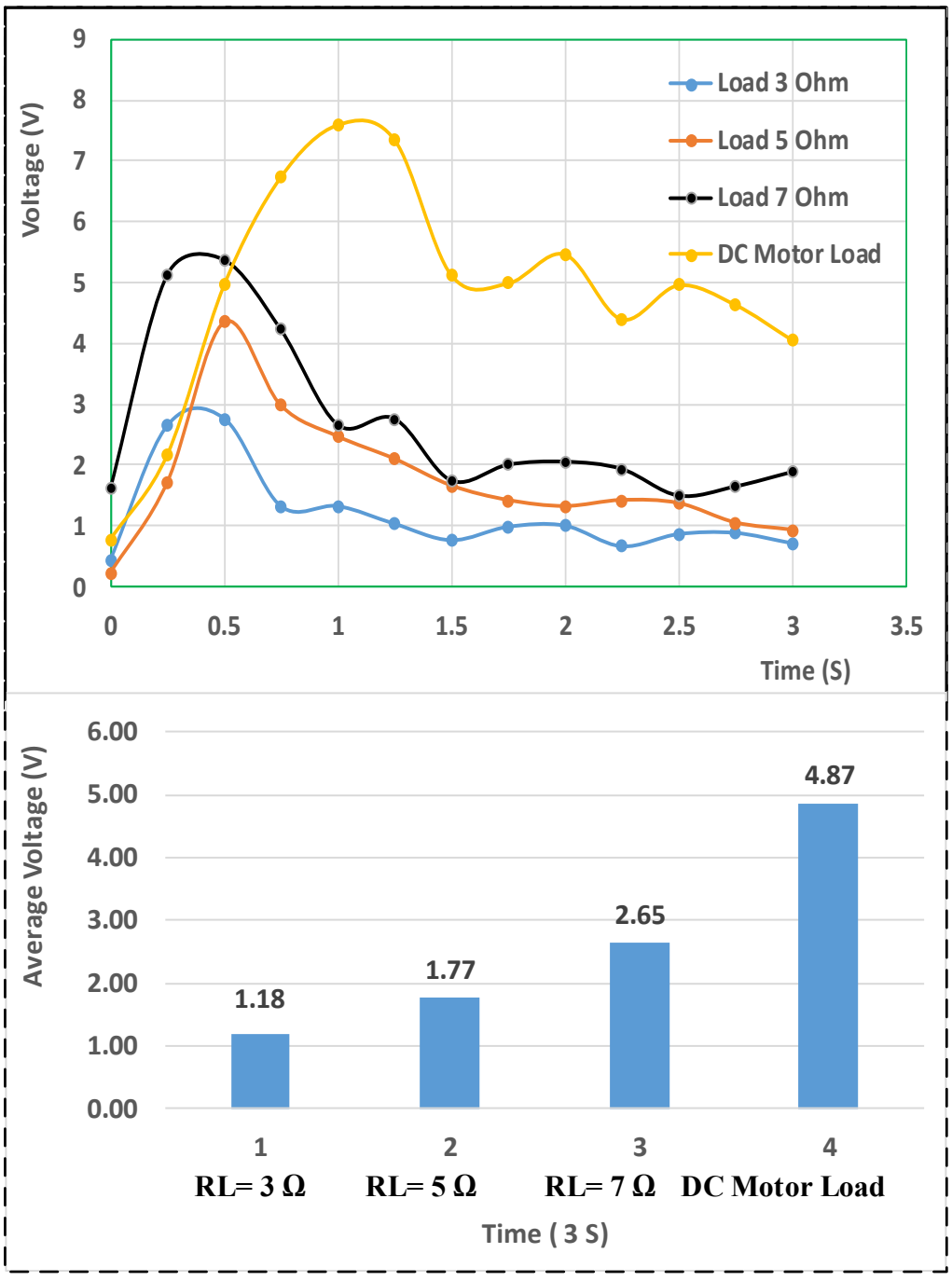

Figure 12. The average voltage comparison between the changing load through 3 second

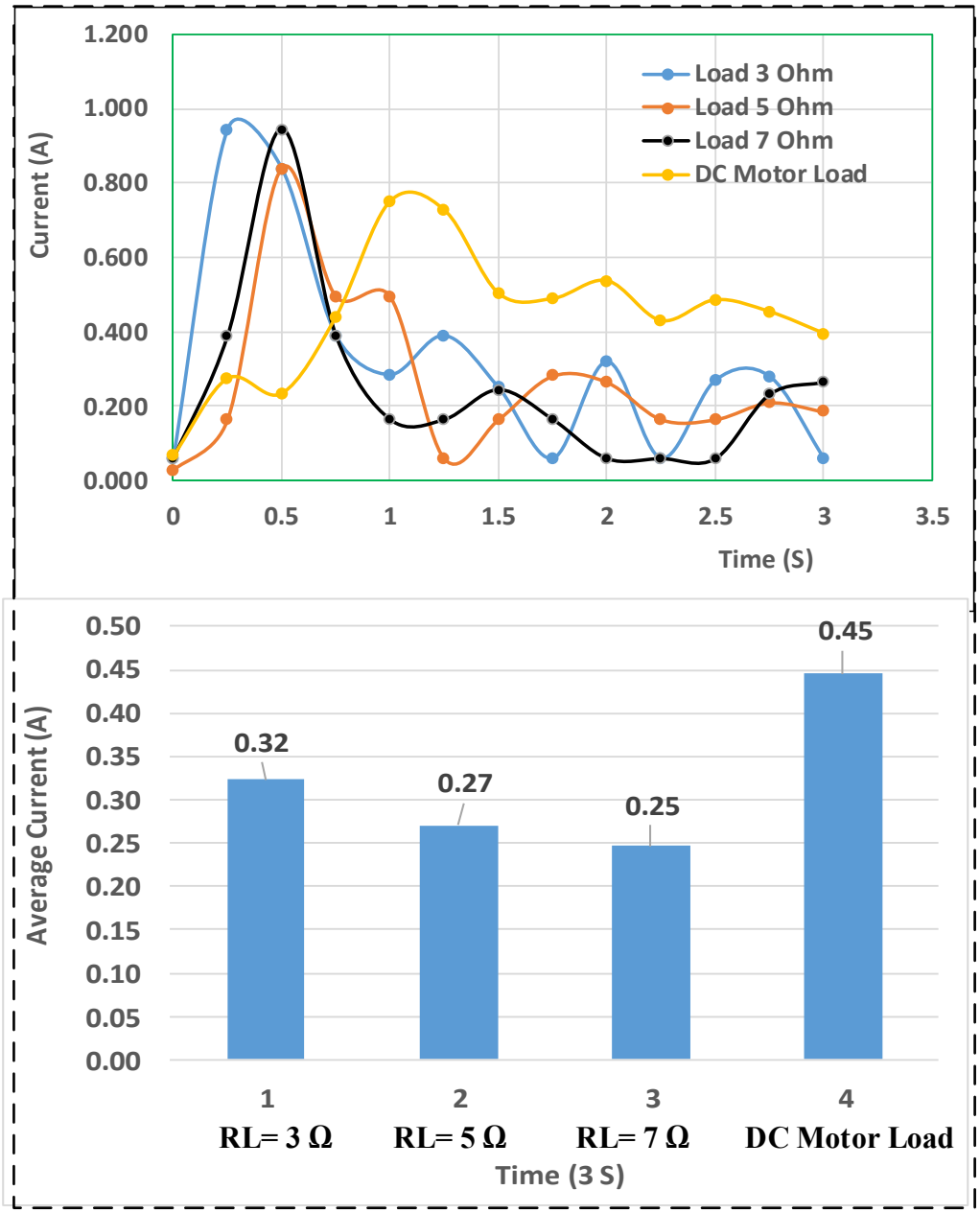

Figure 13. The average current comparison between the changing load through 3 second

The average rotating speed under four changing-load scenarios, where the electrical load was altered every three seconds, is compared in Figure 14. From 1015.38 rpm in Change Load Case 1 to 1033.85 rpm in Case 2, the average rotational speed rose somewhat. In Case 3, the speed then stayed roughly constant at 1033.85 rpm, demonstrating consistent rotational functioning under these two load scenarios. On the other hand, the average rotational speed increased significantly to 1200 rpm in Change Load Case 4. When compared to Case 1, this indicates an increase of almost 18.2%. According to the findings, the rotational speed remained comparatively constant during the first three load circumstances, but it increased under the fourth load condition. The measured speed fluctuation shows how the generator's rotating behavior is affected by shifting electrical loads and operational conditions.

- Change Load Case 1: 1015.38 rpm was the average speed.

- Change Load Case 2: The average speed rose by around 1.82% to 1033.85 rpm.
- Change Load Case 3: In comparison to Case 2, the average speed stayed at around 1033.85 rpm, showing virtually little change.
- Case 4: Change Load When compared to Case 1, the average speed rose to 1200 rpm, or around 18.8%.

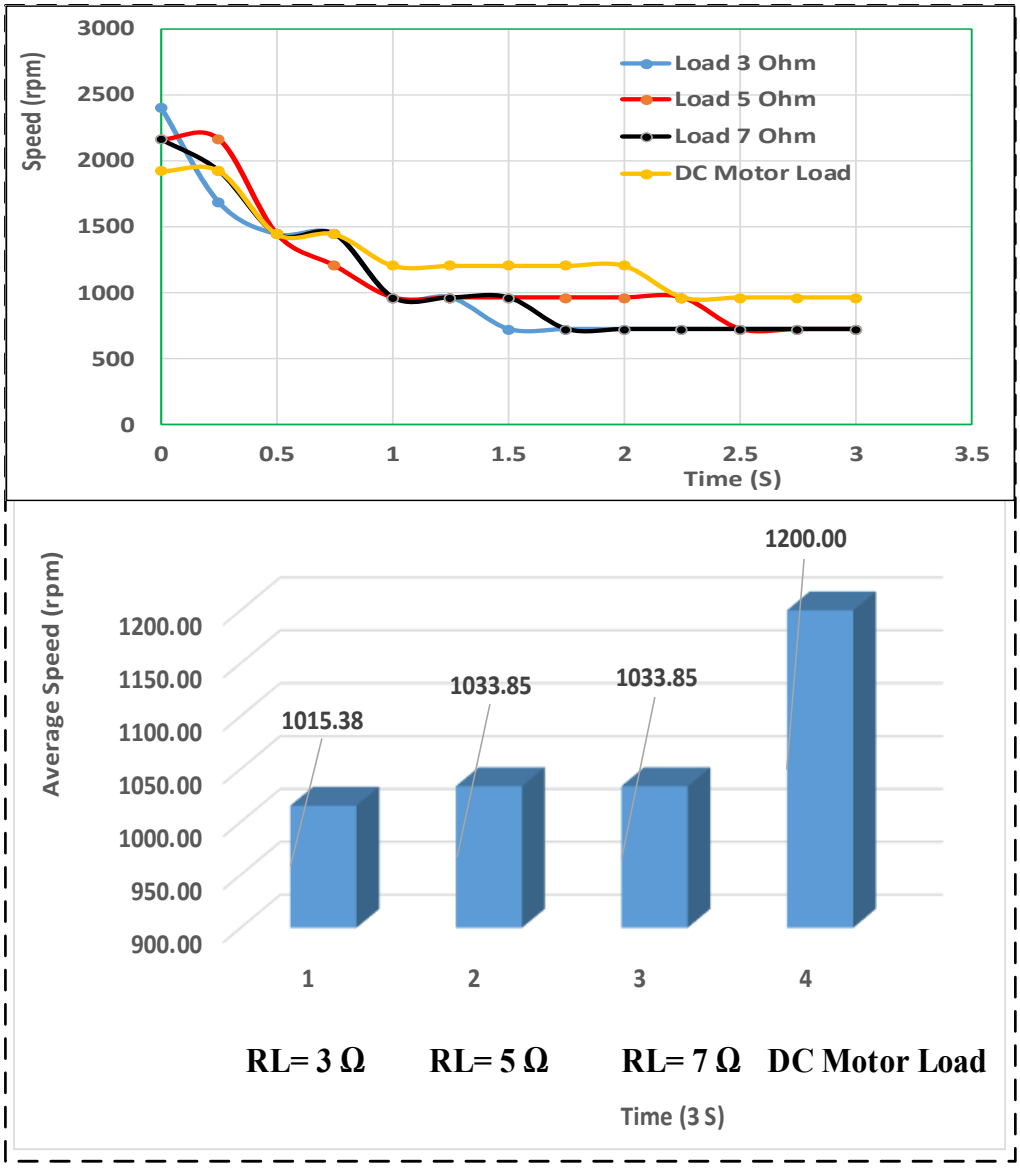

Figure 14. The average speed comparison between the changing load through 3 second

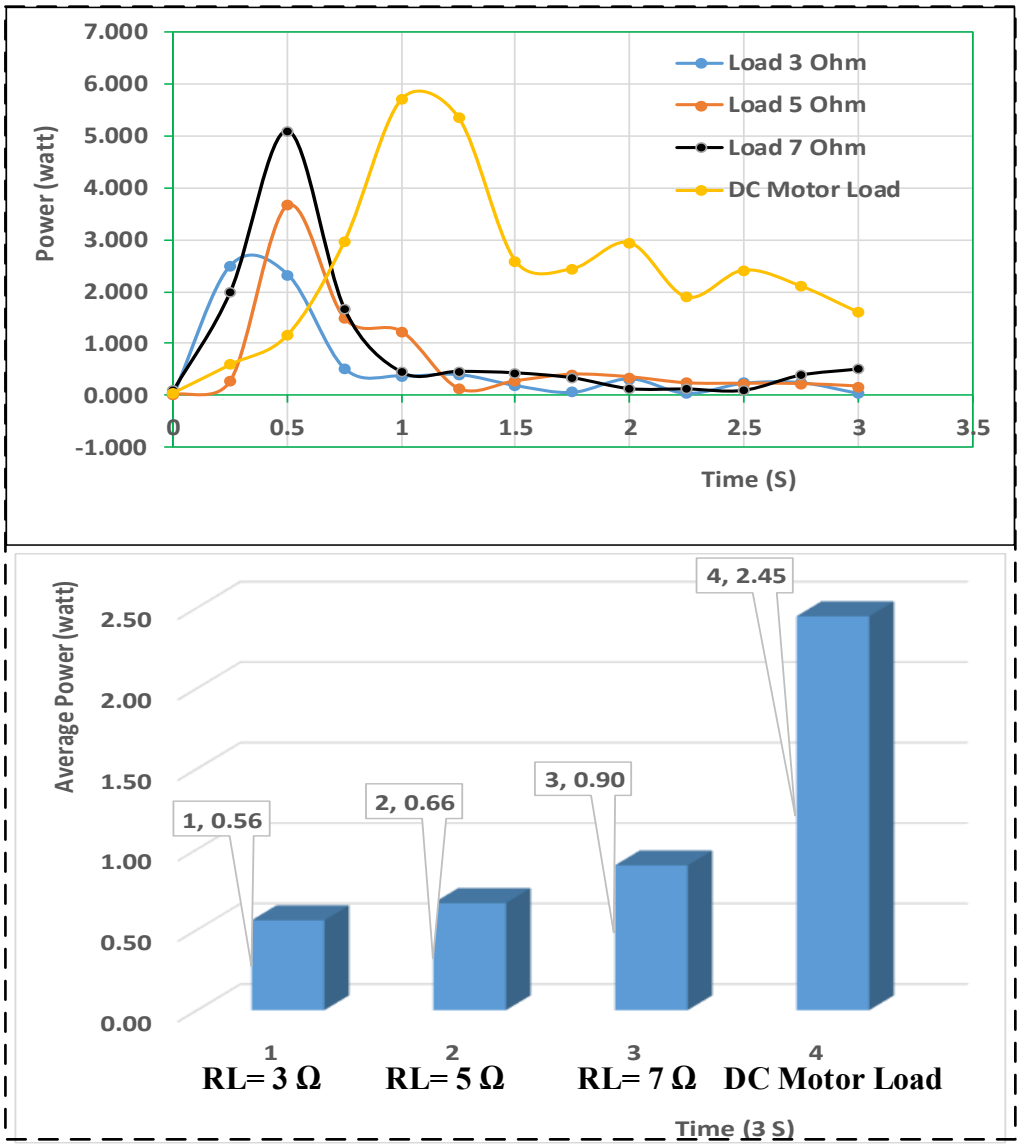

Figure 15. The average power comparison between the changing load through 3 second

The average produced power under four distinct changing-load scenarios, in which the electrical demand was altered every three seconds, is compared in Figure 15. Under the first load condition, the average power was 0.56 W; under the second and third conditions, it increased to 0.66 W and 0.90 W, respectively. The average power rose sharply to 2.45 W under the fourth load scenario. When compared to the initial load state, this indicates an overall increase of about 337.5%. The findings show that the system's power generation performance is significantly impacted by variations in the electrical load. The fourth load condition yielded the highest average power and was linked to the maximum recorded rotating speed of 1200 rpm. As a consequence, the experimental findings show that the applied load and running speed affect the generated power, with the ultimate load condition yielding the maximum electrical power production.

Ten steel blades with two distinct blade thicknesses an initial thickness of 0.5 mm and a later thickness of 1 mm were employed in this study's Tesla turbine. Both groups were subjected to a series of five different pressure levels (6, 7, 8, 9, and 10 bar), while torque was calculated, and the number of revolutions per minute (RPM) whether or not they were under loads well as the

generated values of current, voltage, power, and energy were closely monitored. The findings demonstrated that the power, current, and voltage values from the 1 mm thick feather group were higher than those from the 0.5 mm thick feather group, which went against the original theories [33].

To recover energy from compressed air systems, this study looks at the design, production, and experimental assessment of a low-cost Tesla turbine. To investigate how the type of material affected the turbine's performance characteristics, two distinct disk materials steel and aluminum were investigated. The turbine was incorporated into a compressed air system and tested experimentally under both no-load and electric-load conditions at entry pressures ranging from 2 to 10 bar. Additionally, measured and examined were the turbine's rotational speed and the electrical parameters that resulted, such as voltage, current, and electrical power generated. According to experimental findings, raising the inlet pressure causes the turbine's rotational speed and electrical power to significantly increase [34].

5. Conclusion

performance of the suggested waste-air powered drag turbine. At intervals of three seconds, the electrical load was changed, and the resulting voltage, current, rotating speed, and produced power were recorded. The average rotational speed increased from 1015.38 rpm to 1200 rpm, while the average voltage climbed from 1.18 V under the first load condition to 4.87 V under the fourth condition, according to the data. Additionally, the average produced power rose by almost 337.5%, from 0.56 W to 2.45 W. The final operating state generated the highest measured current of 0.45 A and the maximum power production, despite the fact that the current did not increase continuously with each load condition. These findings demonstrate that the operational parameters and power-generation performance of the suggested system are significantly impacted by the electrical loading state. Overall, the experimental findings show that wasted compressed-air pressure can be used as a source of energy for small-scale electricity generation; however, the overall energy-conversion performance could be enhanced by additional turbine geometry, operating pressure, and electrical loading conditions optimization.

- The findings of the experiment verified that the performance of the suggested waste-air-driven turbine system was greatly impacted by varying the electrical load at intervals of three seconds.
- As the operational load situation changed, the average rotational speed rose from 1015.38 rpm to 1200 rpm.
- The average produced power went from 0.56 W to 2.45 W, while the average voltage went from 1.18 V to 4.87 V.
- The fourth load situation produced the maximum power production, demonstrating enhanced electrical generation under this operating scenario.
- The findings of the experiment show that wasted compressed-air pressure may be used to generate power on a modest scale.
- The produced electrical power and total system efficiency may rise with more advancements in turbine design, operating pressure, and load matching.

Declaration of Conflicts of Interest

Funding: The Authors state that this research did not receive any specific grant from funding agencies in the public, commercial, or not-for-profit sectors.
Conflicts of interest/Competing interests: Nil
Data availability: Yes. I used or generated research data in this study
Availability of data and material: Data files are available upon request

Availability of Data and Materials:

Data files are available upon request

Declarations

Ethical approval
Not applicable.
Consent to participate
YES
Consent to publish
YES

6. References

[1]. Zhao, Y., Teng, S., An, D., & Xi, H. (2025). Performance analysis and optimization of Tesla turbine based on comprehensive operational and structural parameters. Energy Conversion and Management, 332, 119757.

[2]. Zhang, Y., Zhang, S., Peng, H., Tian, Z., Gao, W., & Yang, K. (2023). Thermodynamic analysis of Tesla turbine in Organic Rankine Cycle under two-phase flow conditions. Energy Conversion and Management, 276, 116477.

[3]. Aghagoli, A., & Sorin, M. (2020). CFD modelling and exergy analysis of a heat pump cycle with Tesla turbine using CO2 as a working fluid. Applied Thermal Engineering, 178, 115587.

[4]. Talluri, L., Dumont, O., Manfrida, G., Lemort, V., & Fiaschi, D. (2020). Experimental investigation of an Organic Rankine Cycle Tesla turbine working with R1233zd (E). Applied Thermal Engineering, 174, 115293.

[5]. Teng, S., Li, L., Yan, C., An, D., Zhao, Y., & Xi, H. (2025). Multi-parameter experimental study of a tesla turbine applied to an organic Rankine cycle system for low-grade heat utilisation. Energy Conversion and Management, 333, 119824.

[6]. Thomazoni, André Luis Ribeiro, Conrado Ermel, Paulo Smith Schneider, Lara Werncke Vieira, Julian David Hunt, Sandro Barros Ferreira, Charles Rech, and Vinicius Santorum Gouvêa. "Influence of operational parameters on the performance of Tesla turbines: Experimental investigation of a small-scale turbine." Energy 261 (2022): 125159.

[7]. Rusin, Krzysztof, Włodzimierz Wróblewski, Emad Hasani Malekshah, Mohammadsadegh Pahlavanzadeh, and Sebastian Rulik. "Extended analytical model of Tesla turbine with advanced modelling of velocity profile in minichannel between corotating disks with consideration of surface roughness." Energy 307 (2024): 132775.

[8]. Kosowski, Krzysztof, Marian Piwowarski, Robert Stępień, and Wojciech Włodarski. "Innovative Tesla turbine devices: Concept, testing and insights." Energy 337 (2025): 138731.

[9]. Pahlavanzadeh, Mohammadsadegh, Krzysztof Rusin, Włodzimierz Wróblewski, and Sebastian Rulik. "Roughness effects on flow in Tesla turbine with parametric adjustment of porous layer model." Physics of Fluids 37, no. 1 (2025).
[10]. Ali Kamran, Muhammad, and Shahryar Manzoor. "Effect of nozzle angle, turbine inlets and mass flow rate on the performance of a bladeless turbine." Proceedings of the Institution of Mechanical Engineers, Part A: Journal of Power and Energy 234, no. 8 (2020): 1101-1107.
[11]. Teng, Shiyang, Liushuai Li, Chunjie Yan, Dou An, Yang Zhao, and Huan Xi. "Multi-parameter experimental study of a tesla turbine applied to an organic Rankine cycle system for low-grade heat utilisation." Energy Conversion and Management 333 (2025): 119824.
[12]. Li, Xinyu, Shiyang Teng, Dou an, Tzu-Chen Hung, and Huan Xi. "Experimental investigation of Tesla turbine under different operating parameters and load conditions using air as working fluid." Energy (2025): 138997.
[13]. Zhao, Yang, Shiyang Teng, Dou An, and Huan Xi. "Performance analysis and optimization of Tesla turbine based on comprehensive operational and structural parameters." Energy Conversion and Management 332 (2025): 119757.
[14]. Zheng, Hao, Yonghong Xu, Hongguang Zhang, Jian Zhang, Fubin Yang, Hailong Yang, Baicheng Liu, and Zhuxian Liu. "Performance study of integrated compressor/expander based on small-scale compressed air energy storage system." Journal of Energy Storage 105 (2025): 114689.
[15]. Jung, Jinwon, Phan Anh Duong, Bo Rim Ryu, and Hokeun Kang. "Using Tesla turbine for waste heat recovery: currents status and future directions." J Adv Mar Eng Technol 47, no. 3 (2023): 105-119.
[16]. Sivaramakrishnaiah, Malayathi, Dhanaraj Savary Nasan, Prabhakar Sharma, Thanh Tuan Le, Minh Ho Tran, Thi Bich Ngoc Nguyen, Phuoc Quy Phong Nguyen, and Viet Dung Tran. "Numerical and experimental investigations on a bladeless turbine: Tesla's cohesion-type innovation." International Journal of Renewable Energy Development 13, no. 1 (2024): 110-121.
[17]. Aghagoli, A., and M. Sorin. "CFD modelling and exergy analysis of a heat pump cycle with Tesla turbine using CO2 as a working fluid." Applied Thermal Engineering 178 (2020): 115587.
[18]. Basri, Ernnie Illyani, Adi Azriff Basri, and Farah Nur Diyana Salim. "Study on the effects of individual pitot tube inlet of a bladeless Tesla microturbine using numerical analysis." CFD Lett 15 (2023): 14-30.
[19]. Qi, Wenjiao, Qinghua Deng, Shuxia Yuan, and Bing Chen. "Advantages of the aerodynamic performance of micro-Tesla turbines." Energy Science & Engineering 11, no. 5 (2023): 1734-1752.
[20]. Hoque, Azizul, Md Ektiyer Saki, Tafsir Mehedi, Sk Hasan Tanvirul Islam, Mazharul Islam, and Zambri Harun. "Design and Development of a Small-Capacity Tesla Turbine for Rural Applications." In 2nd International Seminar of Science and Applied Technology (ISSAT 2021), pp. 362-368. Atlantis Press, 2021.
[21]. Sivaramakrishnaiah, Malayathi, R. Meenakshi Reddy, Annapurreddy Damodara Reddy, A. Ravitheja, Prabhu Paramasivam, Mohamed Yusuf, and Praveen Kumar Kanti. "Numerical analysis of energy dynamics in a bladeless turbine nozzle." International Journal of Low-Carbon Technologies 20 (2025): 1383-1391.
[22]. Hoque, Azizul, Md Ektiyer Saki, Tafsir Mehedi, Sk Hasan Tanvirul Islam, Mazharul Islam, and Zambri Harun. "Design and Development of a Small-Capacity Tesla Turbine for Rural

Applications." In 2nd International Seminar of Science and Applied Technology (ISSAT 2021), pp. 362-368. Atlantis Press, 2021.
[23]. Sheikhnejad, Yahya, João Simões, and Nelson Martins. "Introducing Tesla turbine to enhance energy efficiency of refrigeration cycle." Energy Reports 6 (2020): 358-363.
[24]. Galindo, Yovany, José Núñez, and Alberto Beltrán. "Identifying and mitigating energy losses in Tesla turbines: A study on CFD optimization." Energy Science & Engineering 12, no. 10 (2024): 4090-4100.
[25]. Capata, Roberto, and Alfonso Calabria. "The Tesla Turbine—Design, Simulations, Testing and Proposed Applications: A Technological Review." Eng 7, no. 1 (2026): 30.
[26]. Wang, Qin, Zhengyang Zhu, Wei Chen, and Yang Zhou. "A new type of bladeless turbine for compressed gas energy storage system." Frontiers in Chemistry 10 (2022): 1013473.
[27]. Andres, Jibsam F., and Michael E. Loretero. "Performance of tesla turbine using open flow water source." International Journal of Engineering Research and Technology 12, no. 12 (2019): 2191-2199.
[28]. Bhardwaj, Mayank, Sunil Nain, and Upender Dhull. "An exhaustive review of research and development of Tesla turbine technology." Arabian Journal for Science and Engineering 50, no. 17 (2025): 13549-13580.
[29]. Rusin, K., W. Wróblewski, and S. Rulik. "Efficiency based optimization of a Tesla turbine." Energy 236 (2021): 121448.
[30]. Pacini, Leonardo, Lorenzo Ciappi, Lorenzo Talluri, Daniele Fiaschi, Giampaolo Manfrida, and Jacek Smolka. "Computational investigation of partial admission effects on the flow field of a tesla turbine for ORC applications." Energy 212 (2020): 118687.
[31]. Niknam, Pouriya H., Lorenzo Talluri, Lorenzo Ciappi, and Daniele Fiaschi. "Numerical assessment of a two-phase Tesla turbine: Parametric analysis." Applied Thermal Engineering 197 (2021): 117364.
[32]. Ghareghani, Mohammad Sadegh Moradi, Abolfazl Abdolahifar, and S. M. H. Karimian. "Numerical investigation on the helix angle to smoothen aerodynamic torque output of the 3-PB Darrieus vertical axis wind turbine." Journal of Wind Engineering and Industrial Aerodynamics 234 (2023): 105323.
[33]. El Daheb, H. A., & Mosbah, M. A. (2026). Utilizing a Tesla turbine to recover the air brake systems' wasted pressure and transform it into electrical energy. *Next Research*, 101447.
[34]. Farghaly, M. B., Almohammadi, B. A., Alsharif, A. M., Mosbah, M. A., Hussein, E., & El Daheb, H. A. (2026). Experimental evaluation of a cost-effective tesla turbine for waste air energy recovery in transportation systems. *Scientific Reports*, *16*(1), 15177.
[35]. Kock F, Herwig H. Local entropy production in turbulent shear flows: a high- Reynolds number model with wall functions. Int J Heat Mass Tran 2004;47(10e11):2205e15.
[36]. Zhang F, Appiah D, Hong F, Zhang J, Yuan S, Adu-Poku KA, Wei X. Energy loss evaluation in a side channel pump under different wrapping angles using entropy production method. Int Commun Heat Mass Tran 2020;113.
[37]. Hou H, Zhang Y, Li Z, Jiang T, Zhang J, Xu C. Numerical analysis of entropy production on a LNG cryogenic submerged pump. J Nat Gas Sci Eng 2016;36: 87e96.

Supplementary Files

This is a list of supplementary files associated with this preprint. Click to download.

- comparisonresultplot.xlsx